Aust. J. Phys., 1991, **44**, 495–513

Structural Stability of Perturbed mKdV Solitons

J. Roessler

Department of Physics, University of Tasmania,
G.P.O. Box 252C, Hobart, Tas. 7001, Australia.

Abstract

Periodic perturbations are applied to the homoclinic orbits corresponding to solitons of the modified Korteweg–de Vries (mKdV) equation, which is significant in plasma physics and lattice models. It is observed that for certain distinct frequencies the homoclinic orbits do not split into stable and unstable manifolds, which means absence of horseshoes and chaos. The analysis is performed on a travelling wave reduced form of the mKdV equation both by standard application of the Melnikov method as well as numerical generation of Poincaré maps. In particular, the geometry of the homoclinic orbits and their structural changes under perturbations is investigated.

1. Introduction

As we noted in a previous paper (Roessler 1991), the association between soliton solutions of nonlinear evolution partial differential equations (PDEs) and homoclinic orbits has been exposed in one form or another by various authors (Jeffrey and Kakutani 1972; Holmes and Marsden 1981; Birnir 1988). The present paper is a sequel to this previous work, which discussed the application of the Melnikov method to perturbed travelling wave solutions of the KdV equation. In particular, numerical methods and computer programs used in this previous paper are reemployed. Here we apply Melnikov's method to perturbed travelling wave solitons of the mKdV equation

$$u_t - au^2 u_x - bu_{xxx} = 0\,. \tag{1}$$

Like in the case of the KdV equation, most publications on the mKdV equation in the last two decades have concentrated on properties of the equation itself, such as conservation laws, inverse scattering theory, group structures and transformations between solutions. In the present context it is necessary to briefly review the physical significance of the mKdV equation in connection with plasma physics and solid state lattice models so as to provide some framework for the type of perturbations that are introduced which then permit analysis via Melnikov's theory.

0004-9506/91/050495$05.00

(a) Alfvén Waves in Plasma

Alfvén waves have been studied by Kawahara (1970). In a review of his analysis the following equation is derived:

$$\partial f/\partial t + f^2 \partial f/\partial x = V_0 \mu \partial^3 f/\partial x^3 . \tag{2}$$

This is of course the mKdV equation and the dependent variable f is proportional either to the density or velocity fluctuations due to dispersion of the plasma. The wave solutions of (2) are the Alfvén waves, μ is a constant and V_0 is the phase velocity of an idealised (i.e. nondispersive) Alfvén wave. An external forcing term f_{p} periodic in space and time,

$$f_{\mathrm{p}}(x,t) = \alpha \cos(\omega x - \omega_{\mathrm{p}} t) , \tag{3}$$

provides a periodic perturbation to equation (2). Such a perturbation can be induced by an external electromagnetic field. A term f_{d} of the form

$$f_{\mathrm{d}} = -\nu f_{xx} \tag{4}$$

accounts for dissipation or damping of the Alfvén waves. Adding these two terms to the right side of the equation will, after further reduction, allow the application of Melnikov's theory.

(b) Lattice Waves

By lattice we mean here the atomic structure of solids and the vibrations of the atoms which are usually described by so-called lattice waves. We consider the one-dimensional model consisting of a number of particles each of mass m connected to its two neighbours by two springs. Instead of a spring force proportional to the equilibrium displacement y, say, of the individual particle, Zabusky (1967) considered the nonlinear dependence between spring force F and y:

$$F = \kappa(y \pm \alpha y^{p+1}) , \tag{5}$$

with κ, α, p being positive constants. It was shown by Zabusky that the dynamics of a one-dimensional lattice with a spring force of type (5) can in the continuous limit be reduced to the equation

$$\partial u/\partial t \pm u^p \partial u/\partial x + \mu \partial^3 u/\partial x^3 = 0 ,$$

with $u = \partial y/\partial x$ and μ a constant depending on α and p. Perturbations in the form of mechanical vibrations and dissipation presented in the forms (3) and (4) can be considered for periodic forcing and damping.

For an extensive introduction to the Melnikov method we refer to Greenspan and Holmes (1983), Guckenheimer and Holmes (1984) and Wiggins (1988). Although the present analysis is quite similar to that for the KdV equation, technical aspects in the study of the mKdV system are more involved, as there is considerably more variety in its structure. In Section 2 we reduce the perturbed mKdV system via a travelling wave ansatz to a third-order ordinary differential equation (ODE) and then to a second-order ODE by quadrature which we then solve. Section 3 shows the solutions and their geometry in the corresponding three- and two-dimensional phase spaces. The main result appears in Section 4, where we present the Melnikov integrals for the perturbed soliton solutions and discuss some of the numerical analysis of Poincaré maps of the invariant manifolds. We show the absence of a separation between stable and unstable manifolds for certain ranges of parameter values and for certain perturbation frequencies via computer-generated Poincaré maps of non-splitting manifolds, as well as by disappearing Melnikov distances. Our results are summarised in Section 5. Since the application of the Melnikov method is routine and the evaluation of the Melnikov integrals rather technical and straightforward, they are relegated to the Appendix.

2. Reduction of the mKdV Equation

We begin with the equation

$$-u_t + au^2 u_x + bu_{xxx} + \delta u_{xx} + \alpha \cos(\omega x - \omega_{\mathrm{p}}\, t) = 0\,. \tag{6}$$

This is a mKdV–Burgers equation extended by an external periodic forcing term. A travelling wave ansatz

$$y = x - ct, \qquad c = \omega_{\mathrm{p}}/\omega \tag{7}$$

reduces equation (6) to

$$cu_y + au^2 u_y + bu_{yyy} + \delta u_{yy} + \alpha \cos(\omega y) = 0\,. \tag{8}$$

Redefining units of x and t, the wavespeed c can be normalised to unity without loss of generality. Adopting this convention from now on and integrating (8) gives

$$u + au^3/3 + bu_{yy} + \delta u_y + \alpha \sin(\omega y)/\omega = k_1\,, \tag{9}$$

with k_1 as integration constant. The solutions of (9) for vanishing dissipative and periodic forcing terms ($\alpha = \delta = 0$) are of course the travelling wave solutions of the mKdV equation, which include the solitons. After reintroducing small dissipative and periodic forcing terms ($1 > \alpha$, $\delta > 0$) as perturbations, we have the conditions necessary for the application of Melnikov's method.

3. Wave Solutions of the mKdV Equation and Their Geometry

The similarity of the reduced mKdV equation to the Duffing oscillator with weak feedback control, as studied by Wiggins and Holmes (1987), is worth mentioning, as the unperturbed system of their oscillator can be considered a special case of the following analysis. To be complete, we give the solutions corresponding to saddle connections as well as the ones corresponding to periodic orbits.

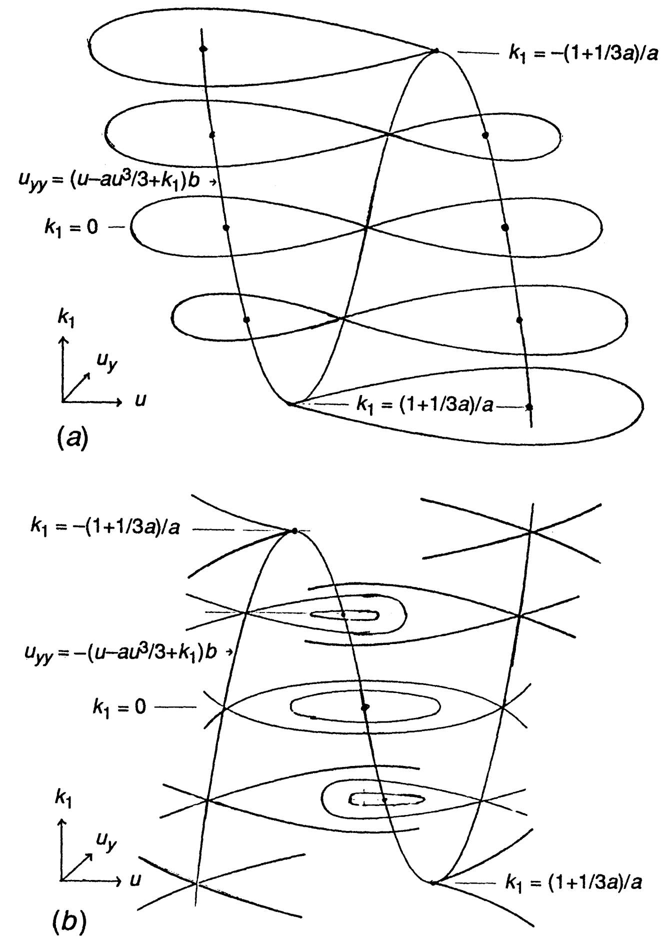

Fig. 1. (*a*) Figure-eight phase portrait in u-u_y-k_1 space. The cubic u_{yy} is given by (9) and yields the set of fixed points. The figure-eight is symmetric for $k_1 = 0$ and degenerates into one loop for $k_1 = \pm(1 + 1/3a)/a$. (*b*) Analogous illustration to (*a*), but for the two saddles phase portrait.

(a) Saddle Connections

Following the approach outlined above, we set $\alpha = \delta = 0$ in (9) and obtain the equation:

$$u + au^3/3 + bu_{yy} = k_1 \,. \tag{10}$$

Multiplying it by u_y, integrating and regrouping terms, leads to

$$\begin{aligned} u_y &= [-u^4 - 6u^2/a + 12k_1\, u/a + 12k_2/a]^{\frac{1}{2}}(a/6b)^{\frac{1}{2}} \\ &= [(u - r_1)(r_2 - u)(r_3 - u)(r_4 - u)]^{\frac{1}{2}}(a/6b)^{\frac{1}{2}} \,, \end{aligned} \tag{11}$$

with the convention on the polynomial roots of $r_1 < r_2 < r_3 < r_4$. We obtain real solutions u such that

$$r_1 \le u \le r_2 < r_3 \le u \le r_4 \qquad \text{for} \quad a,b<0 \quad (a,b>0)\,. \tag{12}$$

By adjusting the integration constant k_2 we can obtain $r_2 = r_3$ which will show up in the space spanned by u_y and u as a figure-eight phase portrait, i.e. two homoclinic loops connected to one saddle. This is equivalent to the unperturbed case in the Duffing system analysed by Wiggins and Holmes (1988) and Fig. 1a illustrates this case for various values of k_1. We will abbreviate this figure-eight case as (f8).

Alternatively, we can change the signs in the roots of (6) such that

$$\begin{aligned} u_y &= [u^4 + 6u^2/a - 12k_1\,u/a - 12k_2/a]^{\frac{1}{2}}(-a/6b)^{\frac{1}{2}} \\ &= [(u-r_1)(u-r_2)(r_3-u)(r_4-u)]^{\frac{1}{2}}(-a/6b)^{\frac{1}{2}}\,. \end{aligned} \tag{13}$$

Now, real solutions are obtained for

$$r_1 < r_2 \le u \le r_3 < r_4 \qquad \text{with} \quad a<0<b \quad (b<0<a)\,. \tag{14}$$

Again by adjusting k_2 so that $r_1 = r_2$ (or $r_3 = r_4$ respectively) we obtain in u_y–u space two saddles and one homoclinic orbit. This geometry, which we abbreviate as (2s), is shown in Fig. 1b for various values of k_1. The two cases described above are the only ones exhibiting saddle connections. Applying the method of quadratures to (11) and (13) gives an implicit representation of the solution $u(y)$ for (f8) and (2s) respectively. Setting $r_2 = r_3$ for the (f8) case and $r_1 = r_2$ for the (2s) case specialises to the solutions corresponding to the four homoclinic orbits possible in these cases. Further algebra and integration extracts the combined solutions expressed in terms of hyperbolic functions,

$$u(y) = C/\{A\cosh[E(y-y_0)] + 2r_s\} + r_s\,, \tag{15}$$

$$A = A_\pm = \pm[-2(r_s^2 + 3/a)]^{\frac{1}{2}}\,, \qquad C = -6(r_s^2 + 1/a)\,,$$

$$E = E_\pm = \pm[-a/b(r_s^2 + 1/a)]^{\frac{1}{2}}\,,$$

$$r_s = \text{position of saddle on } u \text{ axis}\,.$$

$$\text{(f8)}: \qquad a,b<0\,, \qquad 0 \le r_s^2 \le -1/a\,,$$

$$A_-: \textit{left} \text{ loop}\,, \qquad A_+: \textit{right} \text{ loop}\,.$$

$$\text{(2s)}: \qquad a<0<b\,, \qquad -1/a < r_s^2 < -3/a\,,$$

$$A_-: \text{ loop on } \textit{left} \text{ saddle}\,, \qquad A_+: \text{ loop on } \textit{right} \text{ saddle}\,,$$

$$r_s \text{ negative} \qquad\qquad\qquad r_s \text{ positive}$$

The heteroclinic limit for (2s) appears when $r_s = \pm[-3/a]^{1/2}$. The two saddles at $u = +[-3/a]^{1/2}$ and $u = -[-3/a]^{1/2}$ are connected by two heteroclinic orbits (see Fig. 1*b*). Symmetry about the u and u_y axes and elliptic fixed point in the origin is evident; the heteroclinic solutions are given by

$$u(y) = \pm[-3/a]^{\frac{1}{2}} \tanh[\pm(y-y_0)/(2b)^{\frac{1}{2}}], \tag{16}$$

with

$$-[-3/a]^{\frac{1}{2}} = r_1 = r_2 < u(y) < r_3 = r_4 = +[-3/a]^{\frac{1}{2}}, \qquad k_1 = 0.$$

We note that (16) is *not* the limit of (15) case (2s) above, as $r_s \to \pm[-3/a]^{1/2}$.

(b) Periodic Solutions

The derivation of the periodic solution is similar to the saddle connections, except that the integrals are elliptic. The solutions inside the homoclinic loops are in combined form:

$$u(y) = (r_d - r_c)/[\alpha_s^2 \operatorname{sn}^2\{Q_s(y-y_0), k\} - 1] + r_d, \tag{17}$$

$$Q_s = [(r_4 - r_2)(r_3 - r_1)a/24b]^{\frac{1}{2}},$$

$$\alpha_s^2 = (r_b - r_c)/(r_b - r_d),$$

$$k_2 = (r_b - r_c)(r_a - r_c)/(r_4 - r_2)(r_3 - r_1)$$

$$= \alpha_s^2(r_a - r_d)/(r_a - r_c),$$

where the roots r_a, r_b, r_c, r_d are assigned as follows:

(f8) inside *right* loop :

$$r_a = r_1, \quad r_b = r_4, \quad r_c = r_3, \quad r_d = r_2. \tag{18}$$

(f8) inside *left* loop :

$$r_a = r_3, \quad r_b = r_2, \quad r_c = r_1, \quad r_d = r_4. \tag{19}$$

(2s) inside loop on *right* saddle :

$$r_a = r_1, \quad r_b = r_2, \quad r_c = r_3, \quad r_d = r_4. \tag{20}$$

(2s) inside loop on *left* saddle :

$$r_a = r_4, \quad r_b = r_3, \quad r_c = r_2, \quad r_d = r_1. \tag{21}$$

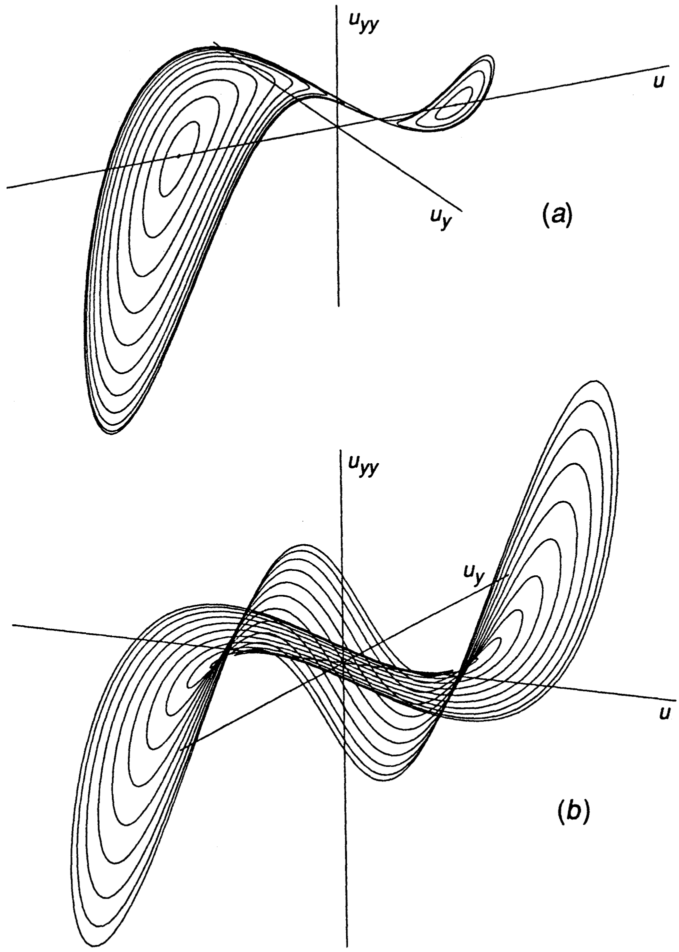

Fig. 2. (*a*) Periodic orbits in u–u_y–u_{yy} phase space enclosed by a pair of homoclinic orbits for (f8) mode. (*b*) Set of homoclinic orbits for (f8) mode in u–u_y–u_{yy} phase space.

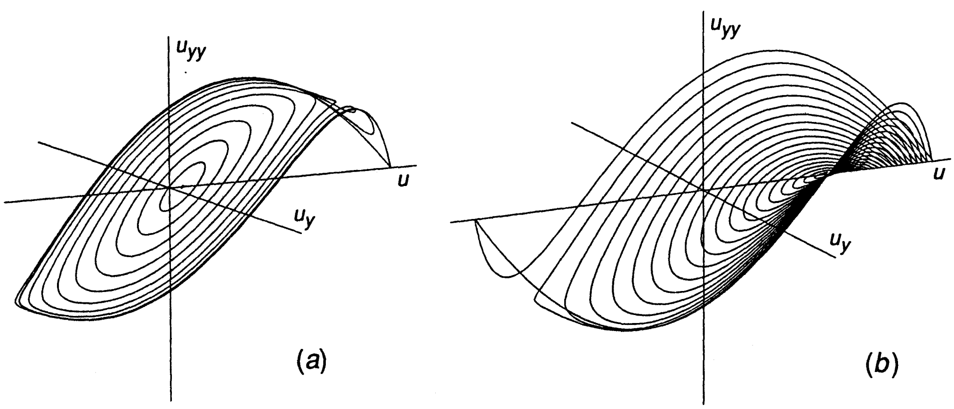

Fig. 3. (*a*) Periodic orbits in u–u_y–u_{yy} phase space enclosed by a homoclinic orbit for (2s) mode. (*b*) Set of homoclinic orbits for (2s) mode in u–u_y–u_{yy} phase space. Note the pair of heteroclinic orbits representing the limit case.

The periodic solutions for (f8) outside the homoclinic orbits are

$$u(y) = [r_4 B + r_1 A + C(r_1 A - r_4 B)]/[B + A + C(A - B)], \tag{22}$$

$$A^2 = [r_4 - (r_2 + r_3)/2]^2 - (r_2 - r_3)^2/4,$$

$$B^2 = [r_1 - (r_2 + r_3)/2]^2 - (r_2 - r_3)^2/4,$$

$$C^2 = \mathrm{cn}\{(y - y_0)[aAB/6b]^{\frac{1}{2}}, k\},$$

$$k^2 = [(r_4 - r_1)^2 - (A - B)^2]/4AB.$$

The periodic solutions for (2s) between heteroclinic saddle connections are

$$u(y) = r_3 \,\mathrm{sn}\{(y - y_0) r_4 [-a/6b]^{\frac{1}{2}}, k\}$$

$$k = r_3/r_4, \qquad r_3^2 + r_4^2 = -1/a. \tag{23}$$

Here sn, cn, dn are Jacobi's elliptic functions and k is their modulus.

(c) Geometry in Phase Space

As already noted, these expressions are solutions of the unperturbed and reduced mKdV equation

$$u_y + au^2 u_y + bu_{yyy} = 0, \tag{24}$$

and an analysis of the corresponding system of three first-order differential equations in u–u_y–u_{yy} phase space reveals the entire u axis as containing all possible fixed points of the system, which are thus degenerate. An analysis of the two-dimensional system obtained from the integrated version of (24),

$$u + au^3/3 + bu_{yy} = k_1, \tag{25}$$

gives the stability type of these fixed points and so allows the construction of the trajectories of the discussed solutions in the u–u_y–u_{yy} phase space. Their geometry is illustrated in Figs 2 and 3 as well as in the earlier Fig. 1. Similar to the case of the KdV equation, the sets of trajectories consisting of concentric periodic orbits enclosed by a homoclinic orbit exist on invariant surfaces P, say, parametrised by k_1 and independent of u_y and whose sections in the u–u_{yy} plane are defined by the cubic (25).

This geometry also helps to explain the role of the integration constant k_1. Since the saddle position r_s must be on the u axis, that is, it has the coordinates $(u = r_s, u_y = 0, u_{yy} = 0)$, it can be seen from (25) to be a function only of a and, more important, of k_1,

$$r_s + ar_s^3/3 = k_1. \tag{26}$$

Therefore k_1 controls the shape of (f8) or (2s) in the phase portrait, whereas k_2 determines the solution within it.

Under perturbations the surfaces P remain invariant, but they are now defined by (9) and, as in the KdV case, each surface P has a slope of value δ in the u_y direction, induced by the dissipation term δu_y. The periodic forcing term induces a y-periodic oscillation of the set of P with frequency ω and amplitude α/b along the u_{yy} axis.

(d) Comparison with the Duffing Problem and the Forced Pendulum

Setting $r_s = k_1 = 0$ leads in the reduced and unperturbed u–u_y phase diagram to symmetry with respect to both u and u_y axes. In (f8) mode this of course reduces the problem to the Duffing system studied extensively and in detail by Greenspan and Holmes (1983) and Guckenheimer and Holmes (1984). In (2s) mode the similarity to the forced pendulum (see e.g. Guckenheimer and Holmes 1984) is only superficial. With the pendulum the two saddles can be identified, which means an inherent periodicity in the phase diagram. In other words, there is a countably infinite number of saddles and pairs of heteroclinic orbits connecting them. On the other hand, the symmetric mKdV (2s) mode has only two saddles and the 'outer' halves of their invariant manifolds are *unbounded.* This difference also manifests itself in the heteroclinic orbit solutions of the type

$$u(t) = \pm 2 \arctan(\sinh t),$$

as given by Guckenheimer and Holmes (1984), clearly different from solution (16).

Wiggins and Holmes (1987) studied the Duffing oscillator with weak feedback control, and without this weak feedback perturbation their system is equivalent to the (unperturbed) (f8) mode. Their perturbation, however, relates to fluctuations of the integration constant k_1. Moreover, both the Duffing system and the pendulum are genuinely two-dimensional systems, whereas the reduced mKdV system is three-dimensional, and although its Melnikov analysis can be reduced to two dimensions, the results of this analysis were justified by reproducing them numerically in the full three-dimensional phase space.

4. Melnikov Functions and Bifurcations

(a) Melnikov Functions

As determined in the Appendix, dissipative perturbations on the reduced mKdV equation (9) contribute the following Melnikov functions for (2s) and (f8) mode respectively:

$$M_{\mathrm{D2s}\pm} = -E_{\pm}\{2r_s A^2/[-C]^{\frac{1}{2}} \tanh^{-1}([-C]^{\frac{1}{2}}/2r_s) + 4r_s^2 + 2C/3\}, \tag{27}$$

$$M_{\mathrm{Df8}\pm} = -E_{\pm}\{2r_s A^2/[C]^{\frac{1}{2}} \tan^{-1}(-[C]^{\frac{1}{2}}/2r_s) + 4r_s^2 + 2C/3\}, \tag{28}$$

where A, C, E and r_s are defined in the homoclinic orbit solution (15). The periodic perturbations contribute for (2s)

$$M_{\mathrm{A2s}\pm}(y_0) = \pm 2[-C]^{\frac{1}{2}} \cos(\omega y_0)\, \pi \sin\{\omega/E \cosh^{-1}(2r_s/A)\}/\{E \sinh(\pi\omega/E)\}, \tag{29}$$

and for (f8)

$$M_{\mathrm{Af8}\pm}(y_0) = \pm 2[C]^{\frac{1}{2}} \cos(\omega y_0)\, \pi \sinh\{\omega/E \cos^{-1}(2r_s/A_+)\}/\{E \sinh(\pi\omega/E)\}, \quad (30)$$

with

$$M_{\mathrm{Af8}-}: \textit{ left loop}, \qquad M_{\mathrm{Af8}+}: \textit{ right loop}.$$

For the heteroclinic solution (16), dissipation and periodic parts M_{hD} and M_{hA} become

$$M_{\mathrm{hD}} = [2/b]^{\frac{1}{2}} 2/a, \quad (31)$$

$$M_{\mathrm{hA}} = [-6b/a]^{\frac{1}{2}} \pi\omega \cos(\omega y_0)/\sinh(\pi\omega[b/2]^{\frac{1}{2}}). \quad (32)$$

(b) Tangencies and Quadratic Zeros

It is clear that the homoclinic Melnikov function $M(y_0)$ has quadratic zeros for $\cos(\omega y_0) = 1$. Therefore, the invariant manifolds W^s and W^u must have tangency points, and we define the tangency ratio $R(\omega)$ for $\alpha = \alpha_c$ and $\delta = \delta_c$:

$$R(\omega) = \alpha_c/\delta_c. \quad (33)$$

This ratio determines the point of bifurcation or transition to chaotic solution for a given ω:

$$\begin{aligned} \alpha/\delta > R(\omega) \quad &\Leftrightarrow \quad W^s \bigwedge W^u \neq 0 \quad \text{(transverse intersection, chaos)}, \\ \alpha/\delta = R(\omega) \quad &\Leftrightarrow \quad W^s \bigwedge W^u \neq 0 \quad \text{(tangency, point of bifurcation)}, \quad (34) \\ \alpha/\delta < R(\omega) \quad &\Leftrightarrow \quad W^s \bigwedge W^u = 0. \end{aligned}$$

For (2s) and (f8) the ratio turns out to be

$$\begin{aligned} R_{2s\pm} = &-\{2r_s A^2/[-C]^{\frac{1}{2}} \tanh^{-1}([-C]^{\frac{1}{2}}/2r_s) + 4r_s^2 + 2C/3\} \\ &\times E^2 \sinh(\pi\omega/E)/(2\pi[-C]^{\frac{1}{2}} \sin\{\omega/E \cosh^{-1}(2r_s/A_\pm)\}), \quad (35) \\ R_{f8\pm} = &-\{2r_s A^2/[C]^{\frac{1}{2}} \tan^{-1}(-[C]^{\frac{1}{2}}/2r_s) + 4r_s^2 + 2C/3\} \\ &\times E^2 \sinh(\pi\omega/E)/(2\pi[C]^{\frac{1}{2}} \sinh\{\omega/E \cos^{-1}(2r_s/A_\pm)\}). \quad (36) \end{aligned}$$

Figs 4 and 5 show $R_{2s\pm}$ and R_{f8+} plotted against r_s and ω. The tangency ratio R_h for this heteroclinic solution is

$$R_h = 2/(\pi b[-3a]^{\frac{1}{2}}) \sinh(\pi\omega[b/2]^{\frac{1}{2}}). \quad (37)$$

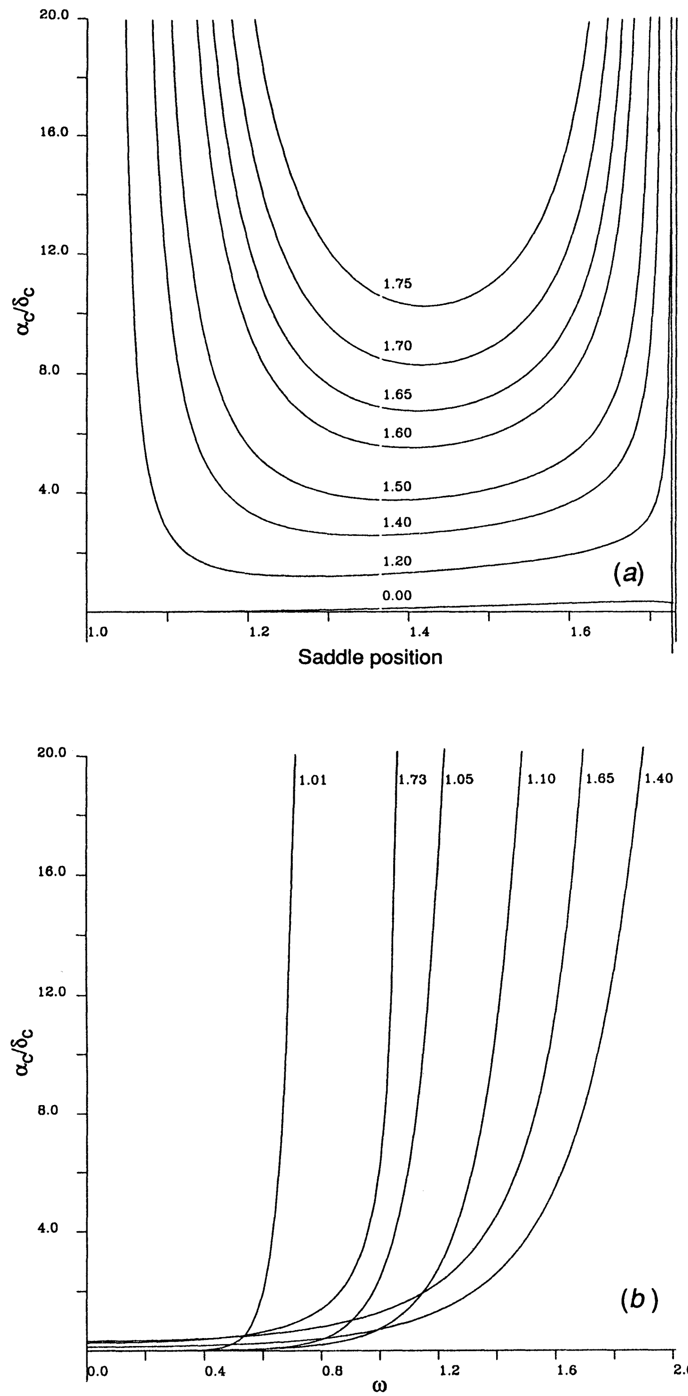

Fig. 4. Bifurcation curves in (2s) mode defined by (35) and evaluated at $a = b = -1$: (*a*) α_c/δ_c versus saddle position for various perturbation frequencies ω; (*b*) α_c/δ_c versus ω for various saddle positions.

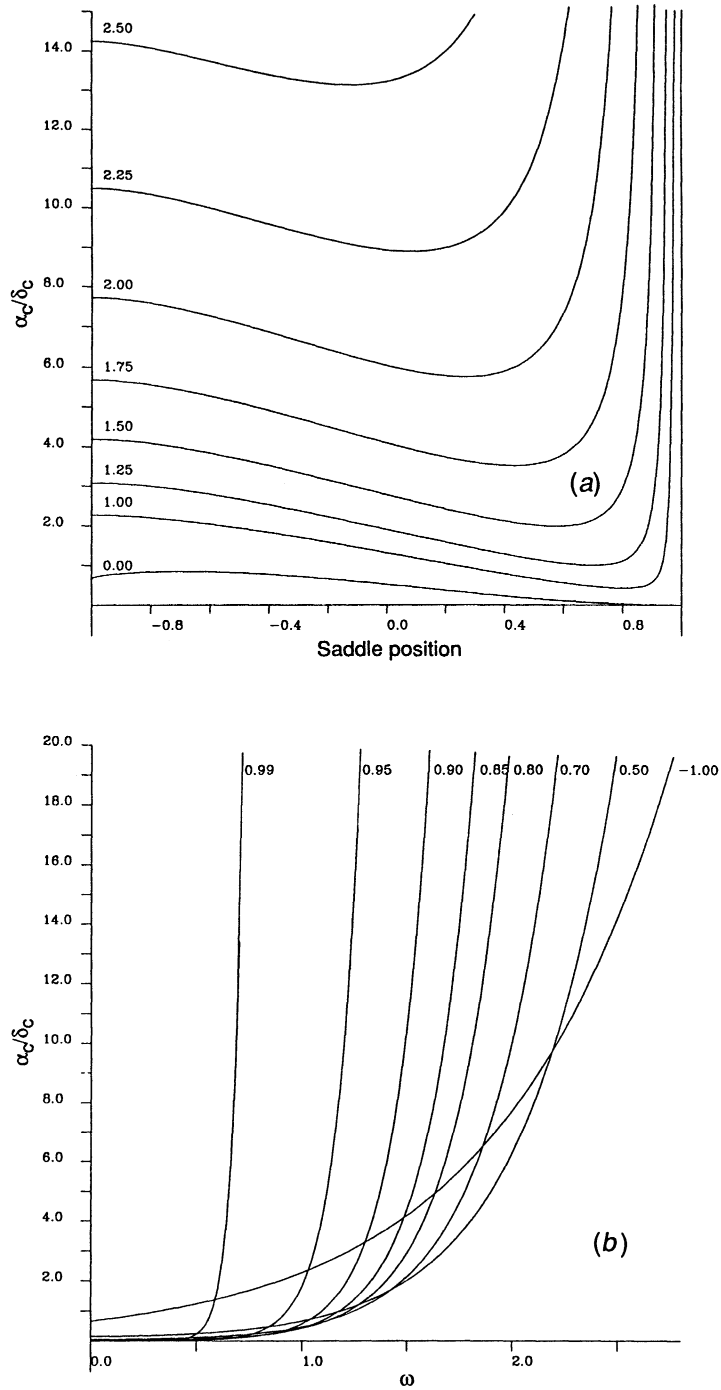

Fig. 5. Bifurcation curves in (f8) mode defined by (36) and evaluated at $a = -1$, $b = 1$: (*a*) α_c/δ_c versus saddle position for various perturbation frequencies ω; (*b*) α_c/δ_c versus ω for various saddle positions.

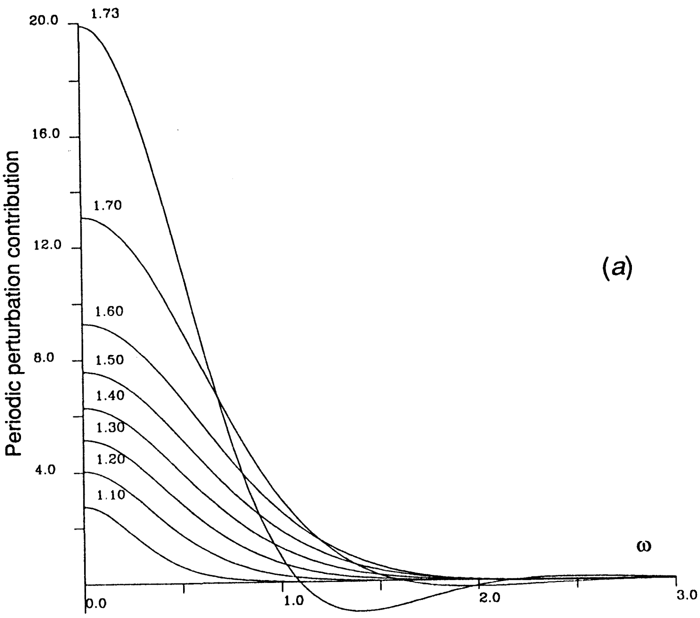

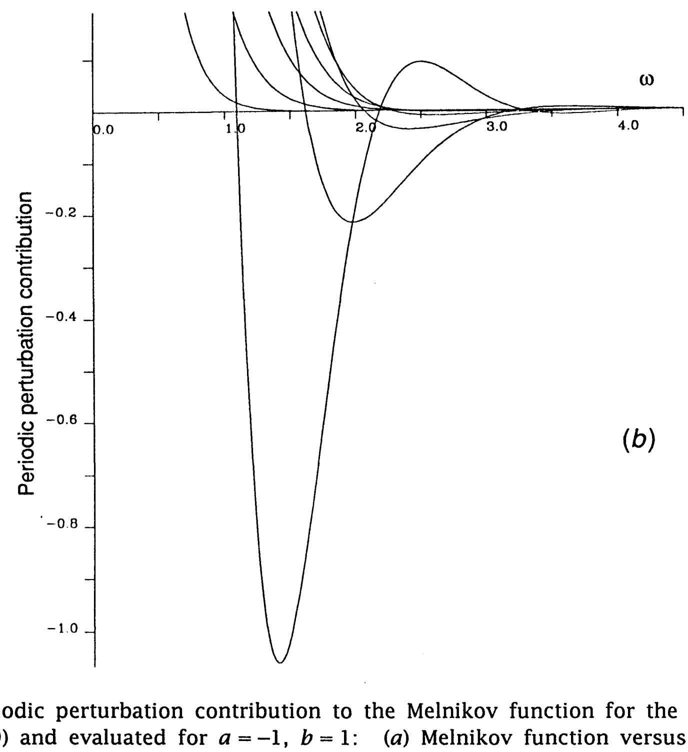

Fig. 6. Periodic perturbation contribution to the Melnikov function for the (2s) mode as given by (29) and evaluated for $a = -1$, $b = 1$: (*a*) Melnikov function versus perturbation frequency ω for various saddle positions; (*b*) Magnification of (*a*) for small and negative values of the Melnikov function. Note the virtual disappearance of the function for values of $\omega \geq 4$.

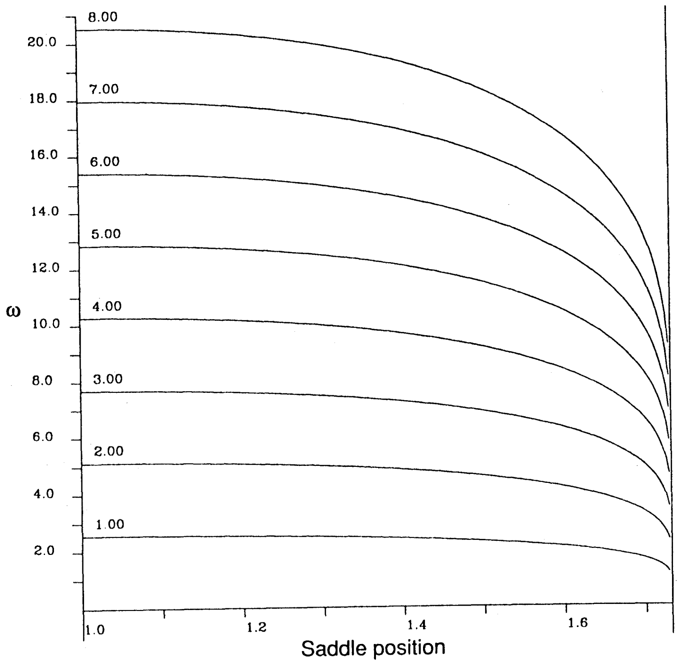

Fig. 7. Zeros of the Melnikov function for Fig. 6 graphed in the saddle position–ω plane.

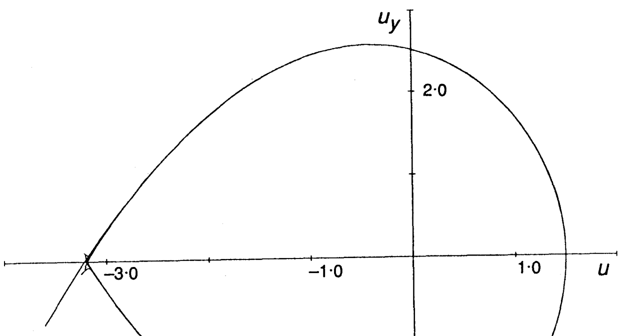

Fig. 8. Invariant manifolds for the (2s) mode projected into the u–u_y plane for $a = -0 \cdot 25$, $b = 0 \cdot 5$, saddle at $u = -3 \cdot 2$, $\alpha = 0 \cdot 3$, $\delta = 0$ and $\omega = 2 \cdot 92$, which is a critical perturbation frequency value with vanishing periodic part of the Melnikov function. Except for a small neighbourhood about the saddle the manifolds overlay exactly within accuracy of the diagram.

(c) Critical Perturbation Frequencies in (2s) Mode

As can be seen from (27), $M_{A2s\pm}$ vanishes independently of y_0 if the perturbation frequency assumes multiples of a certain critical value ω_c such that

$$\sin\{\omega_c/E\cosh^{-1}(2r_s/A)\} = 0\,. \tag{38}$$

This behaviour is illustrated in Figs 6 and 7 and is also verified numerically in Fig. 8. Moreover, Fig. 6 in particular exhibits a rapid decline of the amplitude of $|M_{A2s\pm}|$ with increasing perturbation frequency ω. This virtual disappearance of the periodic part of the Melnikov function for higher perturbation frequencies holds of course for all coefficient values in the mKdV equation in (2s) mode. It is evident from the Melnikov theory that this periodic part of the Melnikov integral is responsible for the transversal intersections and quadratic zeros of the invariant manifolds. According to the Smale–Birkhoff homoclinic theorem, transversal intersections of invariant manifolds are crucial for the formation of Smale horseshoes and the generation of chaos. The homoclinic orbit will survive for certain discrete forcing frequencies and multiples thereof and for all practical intents and purposes for larger frequencies as well, as illustrated by Fig. 6. Transversal intersections will therefore not exist at these critical frequencies and the system cannot display chaos or unbounded growth in the absence of external dissipation. This is supported by numerics as illustrated in Fig. 8, which shows an intact homoclinic orbit under periodic perturbation at the critical forcing frequency $\omega_c = 2\cdot 92$, but without external damping ($\delta = 0$).

(d) Effect of Lower Perturbation Frequencies and Dissipation for (2s)

As can be inferred from Fig. 6 and numerical Poincaré maps, the invariant manifolds split for perturbations with small frequencies. This leads to the formation of horseshoes and transition to chaos as defined by (34) and familiar from the Duffing system. The effect of dissipation is also explained by (34); however, at the critical forcing frequencies the manifolds react to dissipation as if periodic forcing were absent. That is, they split without any intersections or tangencies.

(e) Comparison with Numerics

As with the KdV system (Roessler 1991), the tangency ratios for the mKdV system as given by (35)–(37) are in good agreement with numerically determined tangencies between stable and unstable manifolds of the three-dimensional systems. However, this good agreement breaks down for manifolds relating to relatively small unperturbed homoclinic orbits, that is, for saddles close to the saddle-centre merging points, and for manifolds in the (2s) mode close to the heteroclinic limit. These cases correspond to the regions close to the poles in Figs 4*a* and 5*a*. In these regions the applicability of the first-order Melnikov method becomes questionable, as is evidenced by the large perturbation amplitudes α. The important phenomenon of a vanishing Melnikov distance relating to the periodic perturbation for the mKdV case in (2s) mode is corroborated in Fig. 8 for the critical perturbation frequency $\omega = 2\cdot 92$. Except for a small neighbourhood around the saddle, the invariant manifolds overlay exactly within the accuracy of the graph.

5. Summary

The important result is clearly the stability of the homoclinic orbit under periodic perturbations with certain frequencies and multiples thereof in (2s) mode. Since this phenomenon is manifested both by Melnikov analysis and the numerical generation of Poincaré maps for the invariant manifolds, it cannot be simply attributed to first-order approximations or numerical errors. Although the (2s) system is only a minor variation on the Duffing or (f8) system, this phenomenon does not exist for these or any other known systems exhibiting saddle connections and seems therefore rather unique to the reduced mKdV system in (2s) mode. Moreover, Fig. 6 shows that M_{A2s} becomes negligibly small for high enough frequencies, which can be confirmed by Poincaré maps. This implies *the absence of intersections and tangencies between stable and unstable manifolds; the Smale–Birkhoff homoclinic theorem becomes inapplicable at the critical perturbation frequencies ω_c and for all practical purposes at higher perturbation frequencies as well.* As a consequence, horseshoes and hyperbolic invariant sets with the related chaotic behaviour are *nonexistent*, which has been verified numerically. Another consequence of this vanishing Melnikov distance is that the mKdV system in (2s) displays an intact homoclinic orbit for zero dissipation and perturbation frequencies at the critical values. In other words, the absence of Smale horseshoes and manifold splitting means that the homoclinic orbit survives at these frequencies and merely oscillates with them. This implies structural stability for the homoclinic orbit at these frequency values but structural instability at other frequency values, i.e. almost everywhere in parameter space.

The interpretation in the soliton picture would be that of a breather or bion, or an oscillating soliton. The unperturbed mKdV equation is known to have breathers; however, in the present case the oscillation frequency is induced by a perturbation. It is also worth noting that this is limited to an appropriately moving frame; according to the wave ansatz (7) and wave speed c normalised to unity, both wave number ω and frequency ω_p of the perturbing wave must be (up to dimension) equal to each other as well as to the critical frequencies in order to create an oscillating soliton. More precisely, a normalised wave speed redefines time and length units such that a perturbation has the same number of periods per length unit as per time unit. If this number of periods is at a certain critical value or multiples thereof, the soliton will not become chaotic; in the presence of dissipation it will damp out and in the absence of dissipation it will oscillate with the perturbation frequency, but without energy absorption. This last conclusion follows from the fact that the homoclinic orbit stays intact and is therefore not subjected to the hyperbolic stretching (and ensuing unbounded growth) in the neighbourhood of the saddle, as would be the case for a split stable and unstable manifold.

Finally, we note that the (2s) mode is possible for the case of lattice waves as discussed in the Introduction if the minus sign is chosen in the expression for the spring force (5), and for Alfvén plasma waves (2) if the wave speed V_0 and constant μ are of different sign. Solitons which survive wave-type perturbations of certain frequencies can therefore be expected in these models.

Acknowledgments

The author appreciates the advice and many useful discussions with Professor R. Delbourgo, especially in connection with the special functions appearing in the evaluations of the Melnikov integrals.

References

Birnir, B. (1988). *Physica* D **19**, 238.
Byrd, P. F., and Friedman, M. D. (1972). 'Handbook of Elliptic Integrals for Engineers and Scientists' (Springer: Berlin).
Gradshteyn, I. S., and Ryzhik, I. M. (1965). 'Table of Integrals, Series and Products' (Academic: New York).
Greenspan, B. D., and Holmes, P. (1983). *In* 'Nonlinear Dynamics and Turbulence' (Eds G. I. Barenblatt *et al.*), p. 173 (Pitman: London).
Guckenheimer, J., and Holmes, P. (1984). 'Nonlinear Oscillations, Dynamical Systems and Bifurcations of Vector Fields' (Springer: Berlin).
Holmes, P., and Marsden, J. E. (1981). *Arch. Rat. Mech. Anal.* **76**, 135.
Jeffrey, A., and Kakutani, T. (1972). *SIAM Rev.* **14**, 582.
Kawahara, T. (1970). *J. Phys. Soc. Jpn* **28**, 1321.
Roessler, J. (1991). *Aust. J. Phys.* **44**, 15.
Wiggins, S. (1988). 'Global Bifurcations and Chaos' (Springer: Berlin).
Wiggins, S., and Holmes, P. (1987). *SIAM J. Math. Anal.* **18**, 612.
Zabusky, N. J. (1967). *In* 'Nonlinear Partial Differential Equations' (Ed. W. Ames), p. 223 (Academic: New York).

Appendix

We begin by expressing equation (9) as a two-dimensional first-order system of ODEs:

$$\begin{aligned} u_y &= u_1\,, \\ u_{1y} &= (a^3/3 + u + k_1)/b - \delta u_1 - \alpha \sin(\omega y)/\omega\,, \end{aligned} \tag{A1}$$

after rescaling $\delta \to \delta/b$, $\alpha \to \alpha/b$. As shown by Greenspan and Holmes (1983), for a two-dimensional system such as

$$\begin{gathered} u_t = f_1(u,v) + \epsilon g_1(u,v,t)\,, \\ v_t = f_2(u,v) + \epsilon g_2(u,v,t)\,, \\ u = u(t-t_0)\,, \qquad v = v(t-t_0)\,, \\ g_i(u,v,t) = g_i(u,v,t+T)\,, \qquad i = 1,2\,, \end{gathered} \tag{A2}$$

with ϵ as the perturbation parameter, t_0 a phase factor and T the period of the perturbation (g_1,g_2), the Melnikov integral $M(t_0)$ applicable to the solutions representing the homoclinic orbits of (A2, $\epsilon = 0$) is defined as

$$M(t_0) = \int_{-\infty}^{\infty} (f_1 g_2 - f_2 g_1)\,\mathrm{d}t\,. \tag{A3}$$

Comparison between (A1) and (A2) shows

$$f_1 = u_1 , \qquad \epsilon g_1 = 0 ,$$

$$f_2 = (au^3/3 + u + k_1)/b , \quad \epsilon g_2 = -\delta u_1 - \alpha \sin(\omega y)/\omega . \tag{A4}$$

Introducing one more rescaling, $\epsilon g_2 \to g_2$, and observing that y plays the role of time t, the homoclinic Melnikov integral $M(y_0)$ becomes

$$M(y_0) = -\delta \int_{-\infty}^{\infty} u_y^2 \, dy + \alpha \int_{-\infty}^{\infty} u \cos(\omega y) \, dy$$

$$= -\delta M_D + \alpha M_A . \tag{A5}$$

Substituting the solution (15) and its derivative into (A5), the dissipation part M_D reads

$$M_D = \int_{-\infty}^{\infty} u_y^2 \, dy = (AEC)^2 \int_{-\infty}^{\infty} \sinh^2 E(y-y_0)/[A \cosh E(y-y_0) + 2r_s]^4 \, dy . \tag{A6}$$

Using the substitution $x = E(y - y_0)$ and noting the evenness of the integrand with respect to x, the integral reduces to the form tabulated in Gradshteyn and Ryzhik (1965; p. 346, #3.516.4):

$$M_D = 2E(AC)^2 \int_{-\infty}^{\infty} \sinh^2 x/(A \cosh x + 2r_s)^4 \, dx$$

$$= 2E(AC)^2 K^4 \int_{-\infty}^{\infty} \sinh^2 x/(KA \cosh x + 2Kr_s)^4 \, dx$$

$$= -4E(AD)^2 K^4 \Gamma(2) \Gamma(3/2) Q_2^1(2Kr_s)/[\pi]^{\frac{1}{2}} KA\Gamma(4)$$

$$= -AE[-C] Q_2^1(2r_s/[-C]^{\frac{1}{2}}) . \tag{A7}$$

Here Γ is the gamma function and K is a technical constant determined by comparison of the integral above with Gradshteyn and Ryzhik (1965; p. 346, #3.516.4):

$$K = [-C]^{\frac{1}{2}} = \begin{cases} \text{imaginary for (f8);} & r_s^2 < -1/a \\ \text{real for (2s);} & -1/a < r_s^2 < -3/a . \end{cases} \tag{A8}$$

In (A7) Q_2^1 is the associated Legendre function of the second kind:

$$Q_2^1(z) = -3[z^2 - 1]^{\frac{1}{2}} \tanh^{-1}(1/z) - (3z^2 - 2)/[z^2 - 1]^{\frac{1}{2}} . \tag{A9}$$

For an imaginary argument this reduces to

$$Q_2^1(\mathrm{i}x) = \mathrm{i}\{3[x^2+1]^{\frac{1}{2}}\tan^{-1}(1/x) - (3x^2+2)/[x^2+1]^{\frac{1}{2}}\}. \tag{A10}$$

Therefore M_{D} stays real for (f8) as well and can be expressed in terms of A, C, E and r_{s} (see equation 15) for (2s) and (f8) as

$$M_{\mathrm{D2s}\pm} = -E_{\pm}(2r_{\mathrm{s}}A^2/[-C]^{\frac{1}{2}}\tanh^{-1}([-C]^{\frac{1}{2}}/2r_{\mathrm{s}}) + 4r_{\mathrm{s}}^2 + 2C/3), \tag{A11}$$

$$M_{\mathrm{Df8}\pm} = -E_{\pm}(2r_{\mathrm{s}}A^2/[C]^{\frac{1}{2}}\tan^{-1}(-[C]^{\frac{1}{2}}/2r_{\mathrm{s}}) + 4r_{\mathrm{s}}^2 + 2C/3). \tag{A12}$$

Note that for the left loop (E_-) of $M_{\mathrm{Df8}\pm}$:

$$\lim_{r_{\mathrm{s}}\to +(-)0} \tan^{-1}(-[C]^{\frac{1}{2}}/2r_{\mathrm{s}}) = +(-)\pi/2. \tag{A13}$$

To eliminate this discontinuity, a change of branches of $\tan^{-1}(-[C]^{1/2}/2r_{\mathrm{s}})$ at $r_{\mathrm{s}}=0$ is necessary. Equivalently for the right loop (E_+):

$$\lim_{r_{\mathrm{s}}\to +(-)0} \tan^{-1}(-[C]^{\frac{1}{2}}/2r_{\mathrm{s}}) = -(+)\pi/2. \tag{A14}$$

For the periodic part M_{A} note that we can substitute $U=u-r_{\mathrm{s}}$ for u and shift $y\to y+y_0$:

$$M_{\mathrm{A}}(y_0) = \int_{-\infty}^{\infty} U(y)\cos\omega(y+y_0)\,\mathrm{d}y. \tag{A15}$$

Using the solution (15), $M_{\mathrm{A}}(y_0)$ reduces to

$$M_{\mathrm{A}}(y_0) = -2C\cos(\omega y_0)\int_0^{\infty}\cos(\omega y)/[A\cosh(Ey)+2r_{\mathrm{s}}]\,\mathrm{d}y. \tag{A16}$$

This integral is shown in Gradshteyn and Ryzhik (1965; p. 505, #3.983.1) to have two distinct evaluations:

(1) $\quad 2r_{\mathrm{s}} > A > 0 \quad\Rightarrow\quad 0 < -1/a < r_{\mathrm{s}}^2 \quad\Rightarrow\quad$ (2s) :

$$M_{\mathrm{A2s}\pm}(y_0) = \pm 2[-C]^{\frac{1}{2}}\cos(\omega y_0)\,\pi\,\sin\{\omega/E\cosh^{-1}(2r_{\mathrm{s}}/A)\}/E\sinh(\pi\omega/E); \tag{A17}$$

(2) $\quad |A| > |2r_{\mathrm{s}}| > 0 \quad\Rightarrow\quad 0 < r_{\mathrm{s}}^2 < -1/a \quad\Rightarrow\quad$ (f8) :

$$M_{\mathrm{Af8}\pm}(y_0) = \pm 2[C]^{\frac{1}{2}}\cos(\omega y_0)\,\pi\sinh\{\omega/E\cos^{-1}(2r_{\mathrm{s}}/A_+)\}/E\sinh(\pi\omega/E). \tag{A18}$$

Note that, due to symmetries of the hyperbolic and circular functions, the superscripts or signs on A and E can be omitted or pulled in front of the right sides in (A17) and (A18). Only in the argument of $\cos^{-1}$ in (A18) do the different signs on A change the absolute value of M_{Af8}, corresponding to the two different loops. According to the convention of (15) we therefore distinguish two cases:

$M_{\mathrm{Af8}-}$: *left* loop, $\qquad M_{\mathrm{Af8}+}$: *right* loop.

Manuscript received 1 November 1990, accepted 21 March 1991